Magnetic and dielectric properties of carbon nanotubes with embedded cobalt nanoparticles

Andrey S. Andreev, ariya A. Kazakova, Arcady V. Ishchenko, Alexander G. Selyutin, Olga B. Lapina, Vladimir L. Kuznetsov, Jean-Baptiste D'espinose de Lacaillerie

▶ **To cite this version:**

Andrey S. Andreev, ariya A. Kazakova, Arcady V. Ishchenko, Alexander G. Selyutin, Olga B. Lapina, et al.. Magnetic and dielectric properties of carbon nanotubes with embedded cobalt nanoparticles. Carbon, 2017, 114, pp.39 - 49. 10.1016/j.carbon.2016.11.070 . hal-01418335

HAL Id: hal-01418335
https://hal.science/hal-01418335

Submitted on 16 Dec 2016

HAL is a multi-disciplinary open access archive for the deposit and dissemination of scientific research documents, whether they are published or not. The documents may come from teaching and research institutions in France or abroad, or from public or private research centers.

L'archive ouverte pluridisciplinaire **HAL**, est destinée au dépôt et à la diffusion de documents scientifiques de niveau recherche, publiés ou non, émanant des établissements d'enseignement et de recherche français ou étrangers, des laboratoires publics ou privés.

Magnetic and dielectric properties of carbon nanotubes with embedded cobalt nanoparticles

Andrey S. Andreev [a, b, c], Mariya A. Kazakova [a, b], Arcady V. Ishchenko [a, b], Alexander G. Selyutin [a], Olga B. Lapina [a, b], Vladimir L. Kuznetsov [a, b], Jean-Baptiste d'Espinose de Lacaillerie [c, *]

[a] Boreskov Institute of Catalysis, SB RAS, Lavrentieva 5, Novosibirsk 630090, Russia
[b] Novosibirsk State University, Pirogova 2, Novosibirsk, 630090, Russia
[c] Soft Matter Science and Engineering (SIMM), UMR CNRS 7615, PSL Research University, ESPCI Paris, 75005, Paris, France

ARTICLE INFO

Article history:
Received 7 July 2016
Received in revised form
22 November 2016
Accepted 26 November 2016
Available online 28 November 2016

ABSTRACT

Obtaining stable metal nanoparticles is of high interest for various applications such as catalysis, batteries, supercapacitors and electro-magnetic devices. Cobalt/multi-walled carbon nanotubes (MWCNT) hybrids with an original set of magnetic and electric properties were formed by casting Co nanoparticles (3 − 5 nm) of high aspect ratios within the internal space of MWCNTs. The Co particles localization and size were analyzed by transmission electron microscopy and synchrotron x-ray diffraction. The magnetism of the cobalt nanoparticles was probed by ^{59}Co internal field nuclear magnetic resonance (IF NMR) and their electrical behavior by dielectric spectroscopy. The majority of Co particles were fully metallic. They resisted sintering up to 550 °C. Below 7.5 wt%, the Co was exclusively embedded inside the MWCNT. At higher loading, they coexisted with larger Co outside particles. While nanometer size particles are normally superparamagnetic at room temperature, the confinement of Co within MWCNTs resulted in a ferromagnetism revealed by ^{59}Co IF NMR. This spectroscopy provided original information about the structure, size, and shape anisotropy of the nanoparticles. Finally, the MWCNT modification by Co metal nanoparticles improved the electrical conductivity of polyethylene based composite thus extending the useful frequency band of Co/MWCNT/PE composites for applications requiring lightweight conduction or energy absorption.

with a large diversity of tunable electro-magnetic properties. Finally, the steric control exerted by the well-defined tubular geometry of CNT at the nanoscale opens the possibility to stabilize magnetic NPs of original shapes and structures [28]. This in particular, is a key to control the performance of ternary composites such magnetic NPs/CNT/polymers, a material of tremendous potential for electro-magnetic shielding [29–31].

A common synthetic route to produce Co/CNT composites and hybrids is incipient wetness impregnation with cobalt salt solutions [7,8]. This technique is most simple and easily up scaled. Nevertheless, some more exotic techniques also have been explored [32,33], with specific advantages such as the solvothermal method which can reach Co loadings up to 60 wt% [28,34]. The majority of studies have so far been performed on multi-wall CNT of average diameter in the 50 – 70 nm range [35]. However, multi-wall CNT of smaller diameter are in some cases of higher interest because they exhibit larger surface areas and much larger elastic moduli [36]. Furthermore, smaller tube diameters offer the potential to cast particles of even smaller sizes. An important step of hybrid preparation is the necessity of opening up the CNT to fill their internal space with the Co phase. This can be achieved by treatment with concentrated nitric acid, with the added benefit of creating anchoring sites for Co on the CNTs surface [37,38].

Whatever the chosen synthetic route, the Co precursors loaded on, or in, the CNT (thus forming a true hybrid structure) must be reduced to its metallic state. This is most commonly achieved by exposure to a hydrogen gas flow at elevated temperatures. This reduction procedure is known to proceed in two steps as the spinel Co_3O_4 phase, Co(II) and Co(III), stable under atmospheric conditions, is first reduced into CoO, Co(II), and then into Co(0) metal [39,40]. Since the reverse oxidation reaction occurs easily even at room temperature and is auto-catalytic and pyrophoric in NPs, the Co metal surface is usually passivated by creating a thin oxidized layer through a final treatment with a dilute oxygen stream (1% of O_2 in the inert gas) [28,41]. While this is legitimate when one is concerned only with the shape and internal structure of the metal NPs, it is not clear how much surface state dependent properties such as dielectric properties, magnetism or sintering resistance are modified by this passivation treatment. To study the intrinsic properties of reduced Co metal, it would be preferable to maintain the surface in its native reduced state.

In this paper, the structure and properties of Co metal/multi-wall CNT (Co/MWCNT) hybrids is reported with different Co contents. As the MWCNTs internal geometry is used to template and to stabilize Co magnetic NPs below the 10 nm range (something that is particularly challenging for 3*d* metals), a precise control of the MWCNTs properties is essential. To that respect, we used MWCNTs of 3 – 4 nm internal average diameter and of 4 – 6 nm average wall thickness carefully synthesized and characterized by some of us in previous works [42,43]. The reduction of the precursors is followed by temperature programmed reduction (TPR) and *in situ* synchrotron X-ray diffraction (XRD). High-Resolution Transmission Electron Microscopy (HRTEM), and state-of-the-art ^{59}Co internal field nuclear magnetic resonance (IF-NMR) [44] were combined to probe the shape, structure and magnetism of the Cobalt phase after reduction. IF-NMR is particularly valuable as it reveals quantitatively the different Co metal magnetic NP structures and provides size estimations without exposure to oxygen, information not available by other methods [41,45–51]. In this way, we demonstrate that Co(0) phase in the nanometer range can be cast into the CNTs as ferromagnetic NPs of high aspect ratios or short nanowires. We further show that *in situ* polymerization of polyethylene on Co/MWCNT results in a composite with improved dielectric properties (Fig. 1).

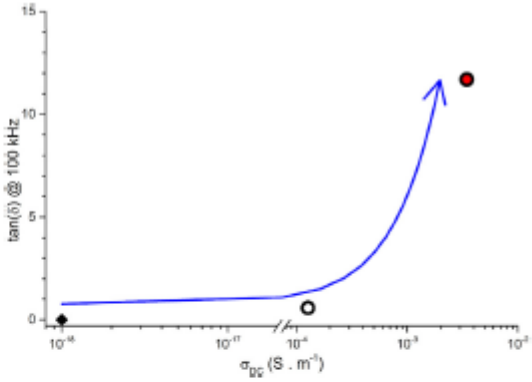

Fig. 1. Comparison of properties of MWCNT polymer composites in view of enhanced absorption properties. The arrow points the improvement toward a high conductivity and high loss material at the largest possible bandwidth (here 100 kHz). Black diamond: typical value for polyethylene; empty circle: MWCNT polyethylene composite, this study; filled circle: Co/MWCNT polyethylene composite, this study. The data correspond to the samples discussed later in Fig. 9. (A colour version of this figure can be viewed online.)

2. Experimental section

2.1. Synthesis of MWCNTs and functionalization

MWCNTs were synthesized by ethylene decomposition over bimetallic Fe-Co catalysts at 680 °C. Conditions were chosen according to ref. [43,52] to target an internal diameter of 3 – 4 nm and a wall thickness of 4 – 6 nm. These characteristics were controlled by statistical analysis of HRTEM images. The Nitrogen BET surface area, measured on the ASAP-2400 Micromeritics instrument, was 305 m^2/g. Carbon nanotube pre-treatment was performed by reflux of 1 – 2 g in an excess of concentrated nitric acid during 90 min. The consequence of this treatment has been evaluated, including by DTA/TGA, in a previous publication [42]. It resulted in the formation of about 0.8 carboxylic groups per 1 nm, while the surface area decreased slightly to 300 m^2/g.

2.2. Co/MWCNT hybrids preparation

Co-containing samples were prepared by incipient wetness impregnation of MWCNTs with aqua solutions of cobalt nitrate [53]. After impregnation for 2 h, the sample precursors were dried at 110 °C for 12 h followed by calcination at 350 °C for 4 h under an argon atmosphere. They were then reduced in a stream of pure hydrogen (40 ml/min) at 350 °C for 3 h with a heating rate of 2 °C/min. Varying the concentration of the cobalt nitrate solutions, samples of 3.5, 7.5, 11.7 and 14.5% Co loading (in weight) were obtained. This was controlled by X-ray fluorescence (XRF) using a sequential spectrometer ARL Perform'X with a Rh anode X-ray tube. The prepared samples were denoted as *x*% Co/MWCNT, the number *x* standing for the cobalt load in weight %. The completeness of the reduction process was verified by temperature programmed reduction (TPR) (Fig. S1). Reduced samples were transferred into NMR ampoules, which were sealed without contact with air immediately after the reduction procedure.

The *in situ* polymerization of polyethylene on Co/MWCNT was carried out as follows. Solvents were purified but reactants were used as received from Sigma Aldrich. Co/MWCNTs (1 g), previously sealed in a glass ampoule, were suspended under an argon atmosphere in heptane containing Triisobutylaluminum (0.4 mmol/g Co/MWCNT) and $TiCl_4$ (0.35 mmol/g Co/MWCNT). The suspension was

dispersed by ultrasound and transferred under Ar atmosphere into a 1 L steel reactor for ethylene polymerization. During the polymerization, the ethylene pressure (3 – 5 atm) and temperature (40 °C) were maintained constant. The reaction was carried out until the desired amount of polyethylene was obtained. After the synthesis, the Co/MWCNT polyethylene composites were stored under air. It will be checked, as exposed below in the Results section, that polyethylene protects efficiently the Co from oxidation.

2.3. *In situ synchrotron X-ray diffraction (XRD)*

The crystal phase transformations of the cobalt phase during the reduction of impregnated MWCNT precursors were monitored *in situ* by XRD on a VEPP 3 Precision Diffractometry station at the Siberian Center of Synchrotron and Terahertz Radiation. The samples were placed in an XRK 900 X-ray reaction chamber (Anton Paar, Austria). Heating was performed from room temperature to 700 °C at a speed of 10 °C/min under a flow of diluted H_2 (H_2 rate of 150 ml/sec). An intermediate stage at 350 °C for 200 min was observed. The X ray patterns were recorded in near real time (60 s per frame) with an OD 3M 350 position sensitive detector in a 2θ range of 33 ° – 65 ° with steps of ~ 0.01 ° (operating wavelength, 0.1731 nm), so as to capture the main reflections of Co, Co_3O_4 and CoO. The X-ray patterns were interpreted using the Topas full profile analysis program. The contribution of the baseline was eliminated by conducting additional experiments on the original nanotubes.

2.4. *High Resolution Transmission Electron Microscopy (HRTEM)*

Morphologies of the CNT supports and of the Co/MWCNT hybrids were characterized using a JEOL JEM-2010 microscope operating at 200 kV accelerating voltage which allows a nominal resolution of 1.4 Å. Sample specimens for TEM studies were prepared by dispersion of the powder in hexane in a glove box under Argon. The hexane suspension was removed from the box and a drop deposited onto a Micro-mesh copper grid and then quickly transferred to the TEM vacuum chamber where it evaporated. The total time of exposure of the hexane suspension to atmosphere was 20 s. The MWCNT mean diameters and Co particle size distributions were estimated from a statistical count of the nanotubes from several frames taken on different parts of the samples.

2.5. *^{59}Co Internal Field nuclear magnetic resonance (IF-NMR)*

All ^{59}Co IF-NMR experiments were carried out using a Bruker Avance NMR console without external magnetic field application, i.e. outside of the NMR magnet, and at ambient temperature. A commercial broadband static low Q NMR probe head with tuning and matching capacitors was used. Although the measurements were not performed *in situ*, the samples were sealed on-line in the glass reactor used for reduction. Thus, during analysis, the samples did not evolve from the state they reached in the reactor, i.e. they were characterized in the same state of reduction and dispersion. The spectra were acquired using the spin-echo Fourier transform point by point method, described elsewhere [49]. The pulse train consisted of two identical pulses of 1 μs duration with an interpulse delay of 8 μs. The number of transients varied from 1 k to 8 k. The sequence repetition rate was 33 Hz due to the very short T_1 relaxation time of ferromagnetic cobalt. Low pulse powers were implemented (< 10 W delivered at the radio-frequency coil) due to the high enhancement factor of metallic Co [54]. All Gaussian peak positions were determined from the "optimal" spectra (see Supporting Information for the definition of an "optimal" spectrum) and were in agreement with previous literature results. Only line widths and line intensities were varied, the peak positions remaining fixed during the spectral decompositions. Small manual deviation from the fixed line positions within 0.2 MHz were allowed to optimize the fit. The details of decomposition procedure can be found elsewhere [54].

2.6. *Complex dielectric permittivity measurement*

The complex dielectric permittivity was measured as a function of frequency and temperature using a HP4284A precision LCR meter in the frequency range from 20 Hz to 1 MHz. The complex effective permittivity was calculated according to the Fresnel equation. All measurements above 1 MHz were performed only at room temperature. The permittivity in the 10 MHz – 20 GHz range was measured using a vector spectrum analyzer (E8363B Agilent Technologies) a coaxial waveguide, an irregular microstrip resonator, and set of rectangular cavity multimode resonators as measuring probes. The permittivity in 200 – 1100 GHz frequency range was measured in a Mach-Zehnder interferometer using continuous radiation generated by backward-wave tubes. The data were normalized to insure continuity between the different frequency ranges.

3. Results and discussion

3.1. *Assessing reduction and sintering by in situ synchrotron XRD*

In situ synchrotron XRD reveals the processes occurring during the reduction of the samples. The actual TPR program was mimicked but for a faster heating rate to 350 °C to allow for a limited available beam-time, as displayed as an inset of Fig. 2.

In Fig. 2, the reduction of the 7.5% Co/MWCNT sample is displayed. The Co phase in the precursor sample initially consisted of a mixture of CoO and Co_3O_4 oxides. As the temperature increased, the characteristic peaks of Co_3O_4 progressively disappeared. The growth of the CoO (111) diffraction line revealed that the first step of Co_3O_4 reduction (from Co_3O_4 to CoO) occurred. Around 320 °C, all reflections from the Co_3O_4 phase disappeared. Simultaneously, the Co^0 (111) peak emerged. Clearly, at this temperature, the second stage of Co^0 reduction (from CoO oxide to Co metal) had started and proceeded during the 350 °C stage. An assessment of the size of the metal particles seen by XRD can be obtained from the breadth of the (111) Co diffraction line using the Scherrer approximation (the face centered cubic (fcc) (111) reflection is used as it is less influenced by stacking faults than the (200) one) [54]. The coherent domain size remained roughly constant at 7 – 8 nm during the 350 °C reduction stage. Sintering was then probed by raising the temperature to 700 °C. Starting at 550 °C, the coherent domain size increased to reach almost 80 nm at the final temperature of 700 °C. Simultaneously, the Co metal reflections dramatically grew. This meant that due to sintering, more and more Co reached the minimum size to diffract coherently and implied that, in the 7.5% Co/MWCNT sample after reduction at 350 °C, a significant number of Co NPs were small enough to escape XRD detection, *i.e.* their size was 5 nm at the very most. Despite their small sizes, these particles resisted sintering until 550 °C, that is close to the Tammann temperature of cobalt metal (604 °C) [55], suggesting a relatively strong metal support interaction between the MWCNT and the Co particles [56].

3.2. *Particles morphology and localization by HRTEM*

HRTEM images of reduced Co/MWCNTs of different Co contents are shown in Fig. 3. The localization and size of the Co NP was clearly revealed and depended on the total Co loading. The 3.5%

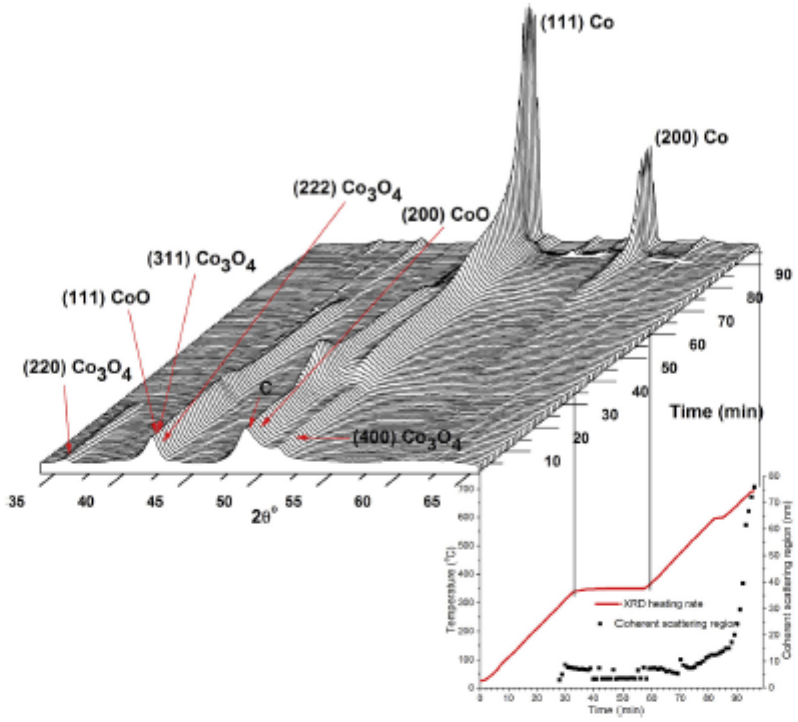

Fig. 2. Time-resolved XRD patterns of the cobalt phases impregnated in MWCNTs (7.5% Co/MWCNT) during reduction under diluted hydrogen and temperature sintering. The operating wavelength is 0.1731 nm. The temperature ramps and coherence size domains derived from the Scherrer approximation are also displayed. Co metal (PDF 15-806), CoO (PDF 48-1719), Co_3O_4 (PDF 42-1467), and C (PDF 43-1104) indexation are shown. The successive reduction of steps of the cobalt spinel into cobalt metal were evidenced but only particles with coherent domain sizes above 5 nm are visible by XRD. Reduction, complete after the 350 °C stage, was followed by temperature sintering up to 700 °C. Sintering, as revealed by the increase of the coherent domain size, occurred only after about 550 °C. (A colour version of this figure can be viewed online.)

sample exhibited only small Co particles inside the CNT channels while, at higher loading a second population of larger sizes appeared outside of the MWCNTs.

The presence of Co NPs inside the MWCNTs thus forming a true Co/MWCNT hybrid was a direct consequence of the nitric acid pretreatment whose effect could be visualized by HRTEM (Fig. S2). Despite, the fact that the nanotubes were closed at their ends, the treatment with nitric acid opened pores within the walls. Consequently, the Co ions could diffuse or be driven inside the tubes during impregnation and drying. Alternatively, the tip of the MWCNTs could have been opened during the nitric acid treatment and closed during the reduction step. In between, during impregnation, the penetration of Co ions would have filled the inner space [38]. The most striking feature from Fig. 3 was that the first population, constrained by the internal dimensions of the nanotubes, was relatively narrow with a constant number average diameter of 3.6 – 4.0 nm and a standard deviation of 1 nm, well in line with the internal nanotube diameter of ~ 4 nm. Furthermore, the localization of the small NPs population inside the MWCNT and the resulting diffusion limitation might explain the resistance to sintering observed by XRD for the small particles in the 7.5% Co/MWCNT hybrid.

As the Co loading increased, the inside population remained constant (Fig. 3) but the size distribution of the outside population increased, widened, and shifted toward higher values reaching a number average of about 21 nm at 14.5% loading. Analysis of the electron diffraction patterns of selected nanoparticles shown in Fig. 4 revealed that, in apparent contradiction with TPR results (Fig. S1) the Co phase present in the HRTEM chamber was partially oxidized. The large particles outside of the tubes had a Co-CoO core-shell structure with a shell thickness of ~ 2 – 3 nm. Consistently, the small particles inside the tubes, being of diameters of less than twice the oxidized shell thickness, were essentially fully oxidized. The discrepancy between the TPR, showing unambiguously that the samples were fully reduced, and electron diffraction data, showing the partial oxidation of the samples analyzed in the HRTEM chamber, likely resulted from a well-known limitation of HRTEM: despite the protection provided by the glove box and then suspension in hexane, the standard sample preparation inevitably resulted in some fractional exposure to air. Nevertheless, this did not alter the validity of the conclusions regarding the particle sizes and localization obtained by HRTEM. Actually, this incidental oxidation revealed that the Co NPs inside the MWCNTs were not particularly protected from oxidation. This behavior contrasted with recent observations by Baaziz et al. [28] concerning clusters (50 ± 5 nm) of Co NPs of similar sizes (5 nm) but confined inside non-porous MWCNTs with a wall thickness an order of magnitude larger (about 20 nm), for which an extremely high resistance to oxidation was reported.

3.3. *Particles sizes, shapes and structures by IF-NMR*

Small particles escape XRD detection, and, as exemplified above, HRTEM is difficult to perform without a minimum level of oxidation. Taking advantage of the magnetic properties of Cobalt metal, these measurements can thus be usefully complemented by ^{59}Co IF-NMR [57]. Before even analyzing the ^{59}Co IF-NMR spectra, the

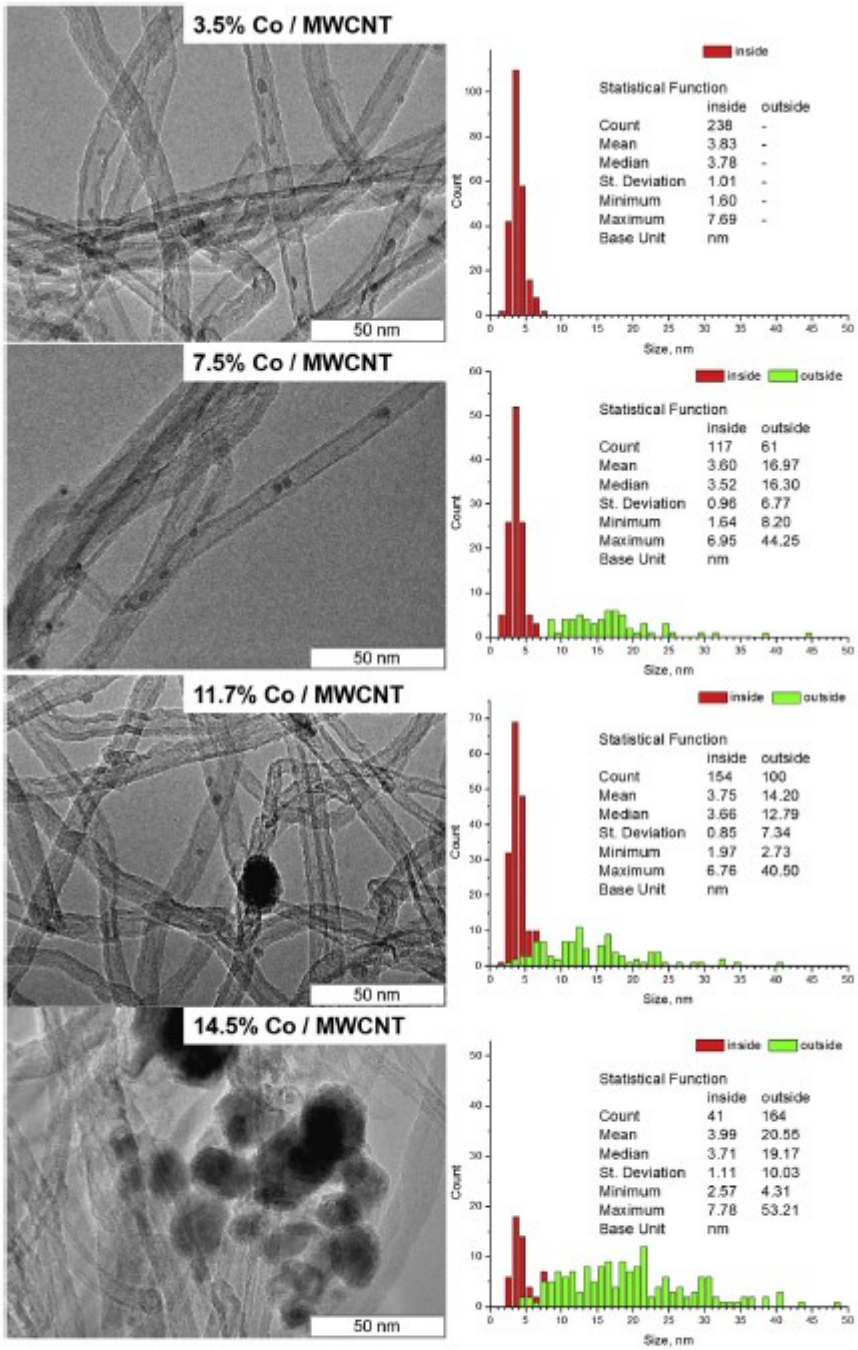

Fig. 3. HRTEM images and particle size histograms of Co/MWCNT hybrids of different Co content (3.5, 7.5, 11.7, and 14.5% Co) after reduction treatment. At low Co loading (3.5%) particles were only present within the nanotube channels; their size histogram (in red) was very sharp and centered below 4 nm, that is with lateral extensions determined by the internal diameter of the MWCNTs. Up to about 10%. Co this population remained predominant but a new population of particles outside of the nanotubes and of larger size appeared (in green). (A colour version of this figure can be viewed online.)

fact that all samples provided a strong ferromagnetic signal was in itself very informative (Fig. 5). First, it demonstrated that the oxidation observed by HRTEM was indeed mostly an artefact and that a significant part, if not all, of the cobalt was indeed metallic in the pristine samples since it is the only one that can exhibit ferromagnetism.

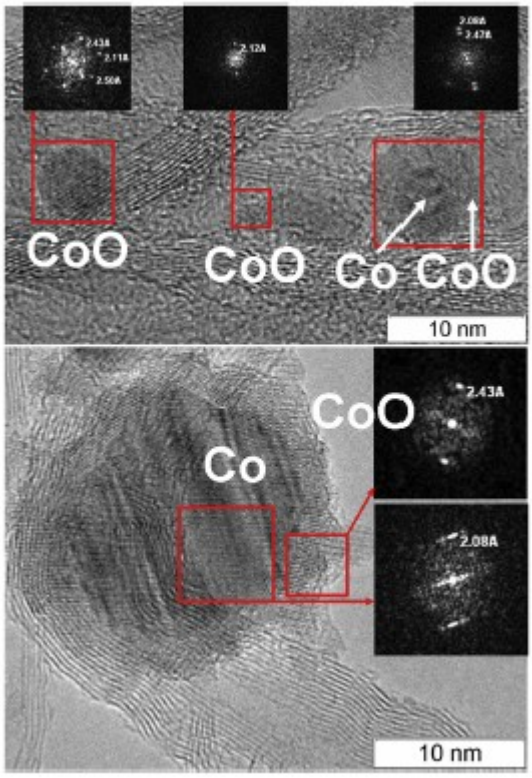

Fig. 4. HRTEM images of 7.5% (above) and 11.7% (below) Co/MWCNT hybrids after reducing treatment with electron diffraction patterns. The particles of the small inside population appeared fully oxidized while the larger outside ones had a Co-CoO core-shell structures. (A colour version of this figure can be viewed online.)

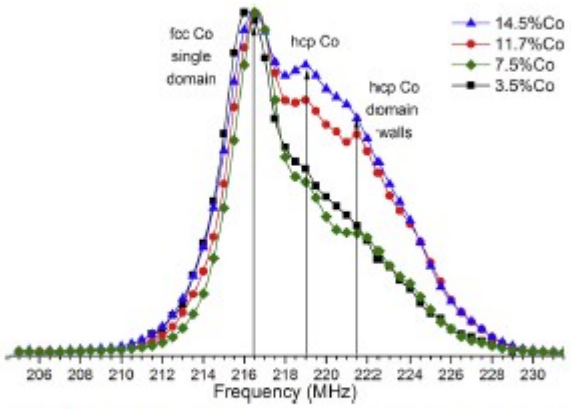

Fig. 5. Optimal ^{59}Co IF-NMR spectra of all Co/MWCNT hybrids (3.5, 7.5, 11.7, 14.5% Co) after reduction. Spectra are normalized to maximum intensity (see Fig. 7 for quantitative analysis). No contribution from multi domain fcc particles could be seen at 213 MHz proving that no fcc particles exceeded the critical domain size at room temperature (50 – 70 nm at the most). For the resonances attributed to the hcp system, a contribution from domain walls occurred despite the small size seen by HRTEM (less than 50 nm in all cases). This was related to the anisotropy of the particles cast inside carbon nanotube channels. (A colour version of this figure can be viewed online.)

Furthermore, for small particles, the occurrence of a ferromagnetic behavior at room temperature is a signature of a significant aspect ratio. According to ref. [58], the blocking temperature T_B for the superpara- to ferro-magnetic transition is given by

$$T_B = \frac{1}{k_B \ln(\tau_m/\tau_0)} V K_{ef}, \quad (1)$$

where V is the particle volume; τ_m is the time of the experimental measurements (10–20 μs in our case); τ_0 is the characteristic relaxation time, in the range of $10^{-9} - 10^{-11}$ s; and K_{ef} is the magnetic anisotropy which results not only from magnetocrystalline anisotropy but also in part from shape anisotropy. For spherical Co particles, $K_{ef} = 5 \times 10^6$ erg·cm^{-3}, a value leading to a critical volume of 1.2×10^2 nm^3 at room temperature, that is to a diameter of about 5 nm. For the 3.5% Co/MWCNT sample, the observation of a ferromagnetic behavior for particles that are all of equivalent diameter inferior to 8 nm established that K_{ef} was significantly lower than in spherical particles, *i.e.* that the Cobalt particles had significant anisotropy caused by the interaction with MWCNTs [59]. Indeed, as shown in Fig. 6 (and Fig. S2), inside the MWCNTs, oblong particles and even nanowires could be detected by HRTEM.

A deeper understanding could be obtained by analyzing the spectral response of the cobalt magnetic NPs. The room temperature corrected ^{59}Co IF-NMR spectrum of the reduced 11.7% Co/MWCNT samples is shown in Fig. 7 together with the variation of the enhancement factor with frequency. The optimal spectra of all the samples are represented in Fig. 5.

Further explanations concerning the notions of optimal and enhancement factor corrections of IF-NMR spectra in ferromagnetic materials are provided in the Supporting Information. Briefly stated, the optimal spectra are obtained by varying the radio-frequency (rf) pulse power and recording for each sampled frequency the point of maximum intensity. The advantage of this representation is that it is independent of the acquisition conditions and is thus fully reproducible. Its disadvantage is that, because the rf field is enhanced differently by different magnetic structures, it is not directly quantitative. A correction by an enhancement factor is thus necessary to quantify the contributions of the different Co ferromagnetic structures. Whatever the chosen representation, the contributions of face centered cubic (fcc) and hexagonal closed-packed (hcp) phases to a ^{59}Co IF-NMR spectrum are very different. The fcc structure being cubic, there is no difference between the resonance frequencies from magnetic domains and from domain walls. The resonances are thus sharp and an easy distinction can be made between the resonances of the fcc multi-domain (213 MHz) and the one from the fcc single-domain particles (216.5 MHz) separated by the contribution of the demagnetization field to the local field. In contrast, in hcp structures, the resonance is distributed over a wide range of frequencies to account for the contributions of Co in domain walls (221.5 MHz), domain wall edges (214 MHz), and domains. The resonance frequency of the latter is poorly defined as it is broadened simultaneously by a large local field anisotropy and by a dispersion of local field values that is not predictable *a priori* since it depends on the particle shapes and sizes [44]. (Note that the resonances of Co in fcc structures with stacking faults cannot be distinguished from the ones in hcp structures as the local environment of Co are similar in both cases).

On this basis, the relative contribution of the fcc and hcp phases was simply obtained by subtracting the contribution of the two fcc 213 MHz and 216.5 MHz resonances from the spectra (see an example in Fig. 6, the results of the decompositions being summarized in Table 1). The first observation is that the multi-domain 213 MHz resonance was systematically absent in our samples. All the fcc particles had thus a single ferromagnetic domain resonating

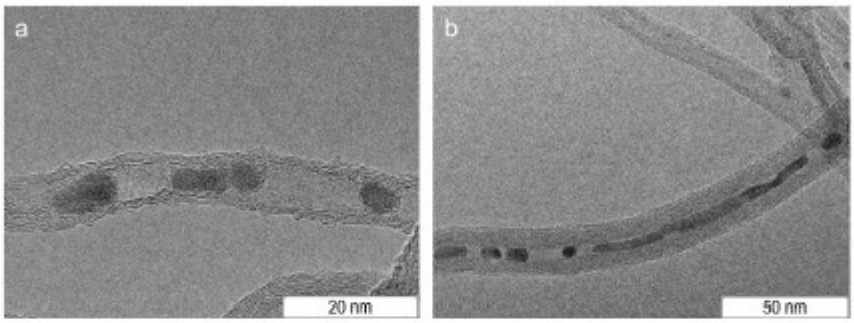

Fig. 6. (**a**) HRTEM image of 3.5% Co/MWCNT showing oblong Co particles within the nanotubes; (**b**) HRTEM image of 7.5% Co/MWCNT showing a Co particle of very high aspect ratio, a Co nanowire inside a carbon nanotube.

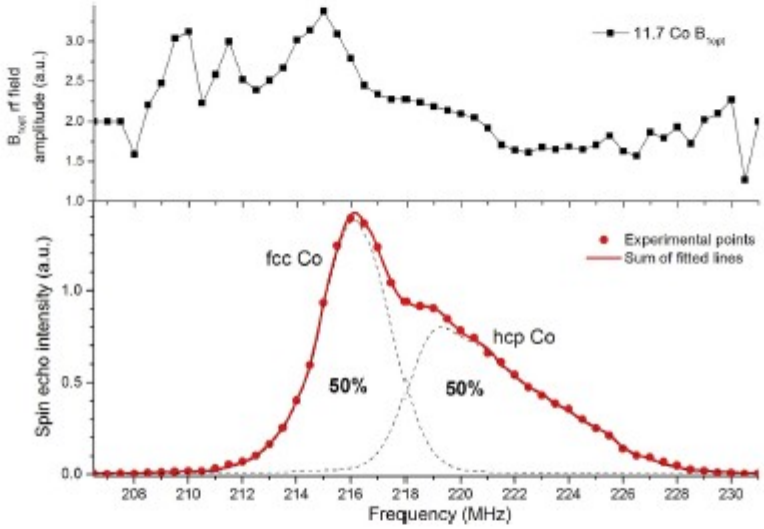

Fig. 7. Corrected ^{59}Co IF-NMR of 11.7% Co/MWCNT hybrid sample after reduction. Also shown is the decomposition into two contributions, fcc and hcp (**bottom**). The optimal B_{1opt} field distribution through the spectrum giving information regarding the relative enhancement factors (**top**). The exact line shape of the hcp resonance was obtained empirically by subtracting the fcc Gaussian line shape. (A colour version of this figure can be viewed online.)

at 216.5 MHz, i.e. they were all smaller than the critical size of Co magnetic domains at room temperature namely ~50 – 70 nm [60]. This was perfectly in line with the HRTEM images where no particles with a diameter larger than 50 nm were observed and very few reported above 30 nm. The second observation was that the relative proportion of the hcp phase increased with the Co loading (Fig. 7 and Table 1). This could be related to the development of the outside population of particles of larger sizes evidenced by HRTEM. Kitakami et al. have evidenced that in small particles, the high-temperature fcc structure is stabilized by the contribution of the surface free energy [61].

Consequently, as the particle sizes increased, the fcc phase was less stable and its proportion decreased with regards to the hcp structure. The growth of the hcp resonance was especially marked around 221.5 MHz (Fig. 5). Such a resonance frequency is typically attributed to Co metal at the center of domain walls in multi domain hcp particles [62,63]. This line was barely resolved in the optimal spectrum representation of Fig. 5 but due to its high enhancement factor was clearly evidenced at low rf field intensity (Fig. S3). The development of magnetic domain walls, possibly not of the same nature as classical Bloch or Néel walls, for particles of effective diameters inferior to the theoretical critical magnetic domain size for spherical particles was further proof that particles of high aspect ratio formed. This 221.5 MHz resonance was thus a signature of the bi-dimensional Co metal structures (nanowires) filling the MWCNTs observed in HRTEM (Fig. 6b).

In summary, we obtained hybrid structure made of cobalt metal nanoparticles within MWCNT. The particles have shapes with a diameter determined by the inner one of the MWCNT, namely circa 4 nm. These particles were of hcp and fcc structures and exhibited ferromagnetism at room temperature despite their small sizes due to their strong anisotropy. For Co loading above 7.5%, additional cobalt nanoparticles were found outside of the nanotubes.

Table 1
hcp/fcc ratio recalculated from the fit of IF-NMR spectra. An example is provided in Fig. 6. The accuracy of the total fcc (hcp) phase determination is ±4%.

Sample Co weight content	3.5%	7.5%	11.7%	14.5%
hcp/fcc ratio	0.75 ± 0.12	0.58 ± 0.10	1.00 ± 0.16	1.17 ± 0.19

3.4. Dielectric properties

Potential applications of this type of hybrid materials relies on their magnetic, dielectric or conducting properties. We have shown that the Co NPs confer an unexpected ferromagnetism to the Co/MWCNT hybrids due to their high shape anisotropy. We now focus on their dielectric permittivity since the magnetic Co particle content is too small to expect a significant change in magnetic permeability (as was verified in the 40 MHz–250 MHz range, data not shown). Pure Co/MWCNT hybrids are not protected from oxidation by air, and thus cannot be used as such. However, their original properties can be conserved when included as filler in a polymer composite. The ideal candidate for utilization as carrier matrixes is polyethylene (PE) due to its plasticity and low melting temperature. However, conventional techniques of composite synthesis (mechanical mixing, dissolution in a melted polymer, *etc.*) are not appropriate when dealing with a highly pyrophoric material such as finely divided Co metal. To overcome these difficulties, polymerization was performed *in situ* directly on Co/MWCNT, as suggested earlier [64].

According to the IF-NMR spectrum in Fig. 8, the Co metal structure is indeed conserved during *in situ* polymerization, therefore structural aspects derived from Co/MWCNT hybrids are valid for ternary (Co/MWCNT) in PE composites.

The electrical response at room temperature of the MWCNT in PE composites with or without Co was in line with percolation theory and typical of a three dimensional conductive network above percolation threshold. The frequency dispersion of dielectric parameters in conductive (here the MWCNT) and insulating (here the PE) composites has been extensively modelled [65]. In Fig. 9, the frequency dispersions of the conductivity

$$\sigma = \varepsilon'' \omega \tag{2}$$

of the dielectric constant relative to the vacuum permittivity ε_0

$$\frac{\varepsilon'}{\varepsilon_0} \tag{3}$$

and of the loss tangent

$$\tan \delta = \frac{\varepsilon''}{\varepsilon'} \tag{4}$$

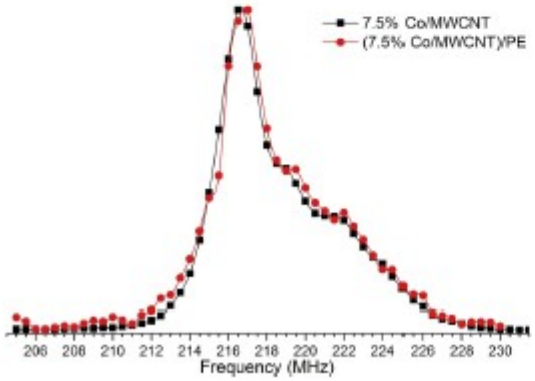

Fig. 8. ^{59}Co IF-NMR spectra of 7.5% Co/MWCNT hybrid sample after reduction (black squares) and in a PE composite. The spectra coincide within experimental errors proving that the Co is efficiently protected from oxidation in the PE matrix. Note that the 7.5% Co/MWCNT in PE composite contain only 14.7% of Co/MWCNT, i.e. Co content inside the PE composite is only about ~ 1%. (A colour version of this figure can be viewed online.)

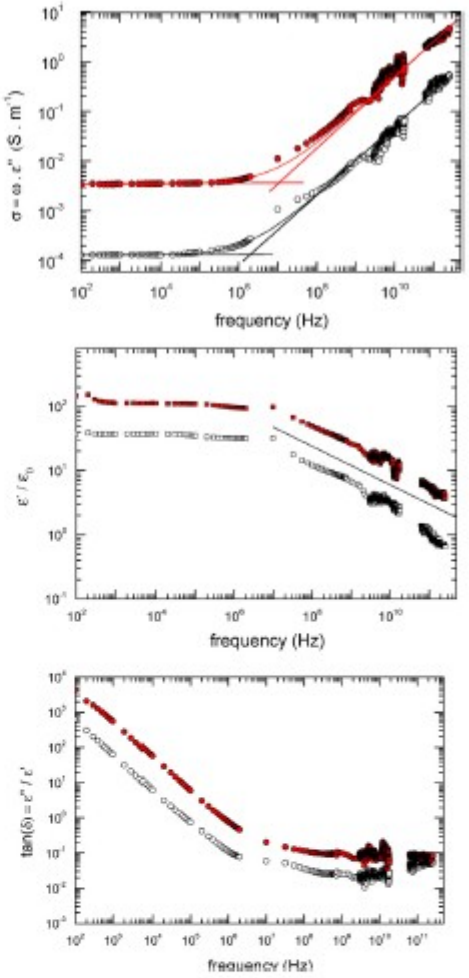

Fig. 9. Room temperature frequency dispersion of electrical conductivity, relative dielectric permittivity and loss tangent sample of similar characteristic but with and without Co nanoparticles. Full symbols, with Co: 13.6% of (7.5% Co/MWCNT) in PE. Empty symbols, without Co: 10.0% of MWCNT in PE. Lines are drawn to show the power laws followed by the conductivity (exponent 0.7) and the dielectric constant (exponent –0.3). Accordingly, the conductivity data were fitted with an Almond-West [66] dispersion law as discussed in the text ($\sigma(\omega) = \sigma_{DC} + \omega A^{(n)}$). (A colour version of this figure can be viewed online.)

of the composites with and without Co are compared. Both samples exhibit the same behavior. Below a crossover frequency, the effective conductivity is constant. Above this crossover frequency, the conductivity increases with frequency while the dielectric constant decreases.

The conductivity is constant at low frequency as the contribution of the DC conductivity, namely the long-range motion of charge carriers, dominates. Beyond a crossover frequency, the effective conductivity and the dielectric constant follow power laws with exponents of about 0.7 and −0.3, respectively. This behavior is thus very close to the prediction of models of 3D random distribution of complex resistors, 0.72 and −0.28 [67–69]. Accordingly, above percolation, the frequency and dielectric constant dispersion beyond the crossover frequency are given by the following scaling laws

Table 2
DC conductivity and crossover frequency between the DC and AC conductivity and corresponding estimation of the variation of the distance to percolation of the samples with and without Co according to equations (8) and (9) and the data for samples without Co, 10.0% of MWCNT in PE, and with Co, 13.6% of (7.5% Co/MWCNT) in PE as provided in Fig. 8.

	Without Co	With Co	$\left(\frac{\lvert\Delta\phi\rvert_{\text{with Co}}}{\lvert\Delta\phi\rvert_{\text{without Co}}}\right)$
σ_{DC} (S. m^{-1})	1.3 10^{-4}	34 10^{-4}	5
ω_c (MHz)	2	10	1.8

$$\sigma(\omega) \propto \omega^{\frac{t}{t+s}} \tag{5}$$

$$\varepsilon'(\omega) \propto \omega^{-\frac{s}{t+s}} \tag{6}$$

$$t \equiv 2 \text{ and } s \equiv 0.8 \tag{7}$$

Interestingly, the value of the dielectric constant is higher for the sample containing Co. This is probably related to the fact that the DC conductivity of this sample is also higher by an order of magnitude in this sample. There is no direct explanation for this as the geometry of the conductive network is not expected to be significantly affected by Co loading of the MWCNT. This can be appreciated by considering the scaling laws of the crossover frequency ω_c, of the DC conductivity σ_{DC}, and of the static permittivity ε_S with respect of the distance to the percolation threshold $\Delta\phi$: [65].

$$\omega_c \propto |\Delta\phi|^{(t+s)} \tag{8}$$

$$\sigma_{DC} = \sigma(\omega \to 0) \propto |\Delta\phi|^t \tag{9}$$

From that, it follows that if the difference in the dielectric properties where solely due to different percolation of the resistor networks, estimation of the ratio of the distance to percolation for both samples through the percolation frequencies or through the DC conductivities should be similar. Experimental estimates are reported in Table 2 from which it appears that the increase in DC conductivity was higher than what would be consistent with a difference in percolation everything remaining equal. In support of this conclusion, we have observed in a previous study of MWCNT/PE composites [64] that doubling the nanotube content inside PE composite from 10 to 20% does not drastically change the dielectric properties. It could thus be safely concluded that it was the presence of Co that was responsible for the enhanced conductivity. The respective contribution of inside and outside particles remains though to be clarified.

The conductivity of elongated conducting heterostructures is determined by the junction resistance at the contacts [70]. This means that the presence of Co was responsible for a significant decrease of the junction resistance between MWCNTs. Enhanced permittivity upon Co loading of carbon nanotubes has been already reported in the literature albeit of lower extent but remains unexplained [35]. In any case, Co loading of the MWCNT resulted in PE composites with a conductivity increased by an order of magnitude. This property is combined with a loss tangent that remained above 10 up to the 100 kHz range, as opposed to only up to the 1 kHz range for the sample without Co. As this was obtained with a minimal modification of the geometry of the percolating MWCNT network, this improvement both in terms of conductivity and absorption bandwidth was obtained without major modifications of the mechanical properties of the composite.

4. Conclusion

Obtaining metal particles in the nanometer range can be experimentally very elaborate. Here, we showed that porous MWCNTs can act as templates to cast Co metal particles of elongated shapes following a simple incipient wetness procedure. Using MWCNTs of small internal diameter allowed the stabilization of particles with a diameter of less than 4 nm but with high aspect ratios. Small metallic particles are not expected to be ferromagnetic at room temperature but because of the tubular geometry into which they were cast, they had a high aspect ratio and magnetic anisotropy factor. This peculiar magnetic property meant that a true ferromagnetic Co/MWCNT nano-hybrid could be synthesized. Depending on the Co loading, particles with diameters an order of magnitude larger could also be deposited on the outside of the tubes. Quantification of each population was performed by HRTEM but this technique does not preserve the oxidation state and phase structure of the particles. On the contrary, IF-NMR provided an original mean to characterize the magnetic NPs in their fully reduced state. Based on the different resonances of ferromagnetic single domains and of domain walls, the absence of large particles and the high aspect ratio of the particles inside the MWCNTs were confirmed up to 7.5 wt% Co loading. Furthermore, the relative amounts of fcc and hcp crystalline phases could be quantified, an information which can be of high interest for catalysis [71] and batteries [12] applications and cannot be obtained by other methods.

The Co magnetic NPs were not protected from oxidation but synchrotron XRD showed that they resisted sintering up to 550 °C. This property is of high interest in catalysis. However, beyond this, the possibility to exploit simultaneously the original electrical transport properties of CNTs and the magnetism of Co NPs also opens the way to use the Co/MWCNT hybrid as a component for polymer composites with new electro-magnetic properties. Although the values of conductivity reached in the present study were not sufficient for effective applications [72], the conductivity was improved by an order of magnitude and the absorption bandwidth in low frequency range by almost two order of magnitude up to 100 kHz. Work is ongoing to understand the respective role of Co particles inside and outside the CNTs, the maximum Co intake inside the CNTs, and how to control the formation of magnetically coupled chains or of long nanowires so as to improve shielding properties in the microwave and terahertz range.

Acknowledgements

The samples preparation and parts of a part of their characterization were made possible by the financial support of the Russian Foundation for Basic Research via grant 16-32-60046 mol_a_dk (Mariya A. Kazakova). Olga B. Lapina and Andrey S. Andreev thank RAS Project V.44.1.17. A. Andreev was also supported in part by a PhD grant from the French Embassy in Moscow and by the Société des Amis de l'ESPCI. The authors thank A. S. Lisitsyn from BIC SB RAS for the TPR analysis and discussion. The authors also thank Professor C. Mény for fruitful discussions regarding IF-NMR. Valentin I. Suslyaev, Evgeniy Yu. Korovin, and Victor A. Zhuravlev are also acknowledged for their help during dielectric measurements, as well as N.V. Semikolenova for Co/MWCNT-PE composite sample preparation.

References

[1] A.-H. Lu, E.L. Salabas, F. Schüth, Magnetic nanoparticles: synthesis, protection, functionalization, and application, Angew. Chem. Int. Ed. 46 (2007) 1222–1244, http://dx.doi.org/10.1002/anie.200602866.

[2] A. Akbarzadeh, M. Samiei, S. Davaran, Magnetic nanoparticles: preparation, physical properties, and applications in biomedicine, Nanoscale Res. Lett. 7 (2012) 144, http://dx.doi.org/10.1186/1556-276X-7-144.

[3] Q.A. Pankhurst, J. Connolly, S.K. Jones, J. Dobson, Applications of magnetic nanoparticles in biomedicine, J. Phys. Appl. Phys. 36 (2003) R167–R181, http://dx.doi.org/10.1088/0022-3727/36/13/201.

[4] A. Ito, M. Shinkai, H. Honda, T. Kobayashi, Medical application of functionalized magnetic nanoparticles, J. Biosci. Bioeng. 100 (2005) 1–11, http://dx.doi.org/10.1263/jbb.100.1.

[5] J. Gao, H. Gu, B. Xu, Multifunctional magnetic nanoparticles: design, synthesis, and biomedical applications, Acc. Chem. Res. 42 (2009) 1097–1107, http://dx.doi.org/10.1021/ar9000026.

[6] S. Bartling, C. Yin, I. Barke, K. Oldenburg, H. Hartmann, V. von Oeynhausen, M.-M. Pohl, K. Houben, E.C. Tyo, S. Seifert, P. Lievens, K.-H. Meiwes-Broer, S. Vajda, Pronounced size dependence in structure and morphology of gas-phase produced, partially oxidized cobalt nanoparticles under catalytic reaction conditions, ACS Nano 9 (2015) 5984–5998, http://dx.doi.org/10.1021/acsnano.5b00791.

[7] H. Zhang, C. Lancelot, W. Chu, J. Hong, A.Y. Khodakov, P.A. Chernavskii, J. Zheng, D. Tong, The nature of cobalt species in carbon nanotubes and their catalytic performance in Fischer–Tropsch reaction, J. Mater. Chem. 19 (2009) 9241–9249, http://dx.doi.org/10.1039/b911355j.

[8] H. Xiong, M.A.M. Motchelaho, M. Moyo, L.L. Jewell, N.J. Coville, Correlating the preparation and performance of cobalt catalysts supported on carbon nanotubes and carbon spheres in the Fischer–Tropsch synthesis, J. Catal. 278 (2011) 26–40, http://dx.doi.org/10.1016/j.jcat.2010.11.010.

[9] S. Lentijo-Mozo, R.P. Tan, C. Garcia-Marcelot, T. Altantzis, P.-F. Fazzini, T. Hungria, B. Cormary, J.R. Gallagher, J.T. Miller, H. Martinez, S. Schrittwieser, J. Schotter, M. Respaud, S. Bals, G. Van Tendeloo, C. Gatel, K. Soulantica, Air- and water-resistant noble metal coated ferromagnetic cobalt nanorods, ACS Nano 9 (2015) 2792–2804, http://dx.doi.org/10.1021/nn506709k.

[10] J. Kim, Y. Piao, T. Hyeon, Multifunctional nanostructured materials for multimodal imaging, and simultaneous imaging and therapy, Chem. Soc. Rev. 38 (2009) 372–390, http://dx.doi.org/10.1039/b709883a.

[11] Y. Xu, M. Mahmood, Z. Li, E. Dervishi, S. Trigwell, V.P. Zharov, N. Ali, V. Saini, A.R. Biris, D. Lupu, D. Boldor, A.S. Biris, Cobalt nanoparticles coated with graphitic shells as localized radio frequency absorbers for cancer therapy, Nanotechnology 19 (2008) 435102, http://dx.doi.org/10.1088/0957-4484/19/43/435102.

[12] C. Rosant, B. Avalle, D. Larcher, L. Dupont, A. Friboulet, J.-M. Tarascon, Biosynthesis of Co3O4 electrode materials by peptide and phage engineering: comprehension and future, Energy Environ. Sci. 5 (2012) 9936–9943, http://dx.doi.org/10.1039/c2ee22234e.

[13] J. Cabana, L. Monconduit, D. Larcher, M.R. Palacín, Beyond intercalation-based Li-ion batteries: the state of the art and challenges of electrode materials reacting through conversion reactions, Adv. Mater. Deerf. Beach Fla 22 (2010) E170–E192, http://dx.doi.org/10.1002/adma.201000717.

[14] T. Fukumaru, T. Fujigaya, N. Nakashima, Development of n-type cobaltocene-encapsulated carbon nanotubes with remarkable thermoelectric property, Sci. Rep. 5 (2015) 7951, http://dx.doi.org/10.1038/srep07951.

[15] S. Iijima, Helical microtubules of graphitic carbon, Nature 354 (1991) 56–58, http://dx.doi.org/10.1038/354056a0.

[16] M. Monthioux, V.L. Kuznetsov, Who should be given the credit for the discovery of carbon nanotubes? Carbon 44 (2006) 1621–1623, http://dx.doi.org/10.1016/j.carbon.2006.03.019.

[17] A. Peigney, C. Laurent, E. Flahaut, R.R. Bacsa, A. Rousset, Specific surface area of carbon nanotubes and bundles of carbon nanotubes, Carbon 39 (2001) 507–514, http://dx.doi.org/10.1016/S0008-6223(00)00155-X.

[18] S. Chakraborty, J. Chattopadhyay, H. Peng, Z. Chen, A. Mukherjee, R.S. Arvidson, R.H. Hauge, W.E. Billups, Surface area measurement of functionalized single-walled carbon nanotubes, J. Phys. Chem. B 110 (2006) 24812–24815, http://dx.doi.org/10.1021/jp065044u.

[19] A.E. Aliev, M.H. Lima, E.M. Silverman, R.H. Baughman, Thermal conductivity of multi-walled carbon nanotube sheets: radiation losses and quenching of phonon modes, Nanotechnology 21 (2010) 035709, http://dx.doi.org/10.1088/0957-4484/21/3/035709.

[20] D.J. Yang, Q. Zhang, G. Chen, S.F. Yoon, J. Ahn, S.G. Wang, Q. Zhou, Q. Wang, J.Q. Li, Thermal conductivity of multiwalled carbon nanotubes, Phys. Rev. B 66 (2002) 165440, http://dx.doi.org/10.1103/PhysRevB.66.165440.

[21] R. Prasher, Thermal boundary resistance and thermal conductivity of multiwalled carbon nanotubes, Phys. Rev. B 77 (2008) 075424, http://dx.doi.org/10.1103/PhysRevB.77.075424.

[22] C.-M. Chang, Y.-L. Liu, Electrical conductivity enhancement of polymer/multiwalled carbon nanotube (MWCNT) composites by thermally-induced defunctionalization of MWCNTs, ACS Appl. Mater. Interfaces 3 (2011) 2204–2208, http://dx.doi.org/10.1021/am200558f.

[23] E.J. Ra, K.H. An, K.K. Kim, S.Y. Jeong, Y.H. Lee, Anisotropic electrical conductivity of MWCNT/PAN nanofiber paper, Chem. Phys. Lett. 413 (2005) 188–193, http://dx.doi.org/10.1016/j.cplett.2005.07.061.

[24] A.V. Eletskii, A.A. Knizhnik, B.V. Potapkin, J.M. Kenny, Electrical characteristics of carbon nanotube-doped composites, Phys. Uspekhi 58 (2015) 209–251, http://dx.doi.org/10.3367/UFNe.0185.201503a.0225.

[25] J.N. Coleman, U. Khan, W.J. Blau, Y.K. Gun'ko, Small but strong: a review of the mechanical properties of carbon nanotube–polymer composites, Carbon 44 (2006) 1624–1652, http://dx.doi.org/10.1016/j.carbon.2006.02.038.

[26] B. Arash, Q. Wang, V.K. Varadan, Mechanical properties of carbon nanotube/polymer composites, Sci. Rep. 4 (2014) 6479, http://dx.doi.org/10.1038/srep06479.

[27] R.S. Ruoff, D. Qian, W.K. Liu, Mechanical properties of carbon nanotubes: theoretical predictions and experimental measurements, Comptes Rendus Phys. 4 (2003) 993–1008, http://dx.doi.org/10.1016/j.crhy.2003.08.001.

[28] W. Baaziz, I. Florea, S. Moldovan, V. Papaefthimiou, S. Zafeiratos, S. Begin-Colin, D. Begin, O. Ersen, C. Pham-Huu, Microscopy investigations of the microstructural change and thermal response of cobalt-based nanoparticles confined inside a carbon nanotube medium, J. Mater Chem. A 3 (2015) 11203–11214, http://dx.doi.org/10.1039/C5TA00283D.

[29] P.Y. Keng, B.Y. Kim, I.-B. Shim, R. Sahoo, P.E. Veneman, N.R. Armstrong, H. Yoo, J.E. Pemberton, M.M. Bull, J.J. Griebel, E.L. Ratcliff, K.G. Nebesny, J. Pyun, Colloidal polymerization of polymer-coated ferromagnetic nanoparticles into cobalt oxide nanowires, ACS Nano 3 (2009) 3143–3157, http://dx.doi.org/10.1021/nn900483w.

[30] L.V. Lutsev, N.E. Kazantseva, I.A. Tchmutin, N.G. Ryvkina, Y.E. Kalinin, A.V. Sitnikoff, Dielectric and magnetic losses of microwave electromagnetic radiation in granular structures with ferromagnetic nanoparticles, J. Phys. Condens. Matter 15 (2003) 3665–3681, http://dx.doi.org/10.1088/0953-8984/15/22/302.

[31] L.V. Lutsev, Spin excitations in granular structures with ferromagnetic nanoparticles, Phys. Solid State 44 (2002) 102–110, http://dx.doi.org/10.1134/1.1434594.

[32] P.M.F.J. Costa, J. Sloan, T. Rutherford, M.L.H. Green, Encapsulation of RexOy clusters within single-walled carbon nanotubes and their in tubulo reduction and sintering to re metal, Chem. Mater. 17 (2005) 6579–6582, http://dx.doi.org/10.1021/cm051020g.

[33] I. Martín-Fabiani, M.-C. García-Gutiérrez, D.R. Rueda, A. Linares, J.J. Hernández, T.A. Ezquerra, M. Reynolds, Crystallization under one-dimensional confinement in alumina nanopores of poly(trimethylene terephthalate) and its composites with single wall carbon nanotubes, ACS Appl. Mater. Interfaces 5 (2013) 5324–5329, http://dx.doi.org/10.1021/am401194p.

[34] W. Baaziz, S. Begin-Colin, B.P. Pichon, I. Florea, O. Ersen, S. Zafeiratos, R. Barbosa, D. Begin, C. Pham-Huu, High-density monodispersed cobalt nanoparticles filled into multiwalled carbon nanotubes, Chem. Mater. 24 (2012) 1549–1551, http://dx.doi.org/10.1021/cm300293h.

[35] H. Lin, H. Zhu, H. Guo, L. Yu, Microwave-absorbing properties of Co-filled carbon nanotubes, Mater. Res. Bull. 43 (2008) 2697–2702, http://dx.doi.org/10.1016/j.materresbull.2007.10.016.

[36] K.V. Elumeeva, V.L. Kuznetsov, A.V. Ischenko, R. Smajda, M. Spina, L. Forro, A. Magrez, Reinforcement of CVD grown multi-walled carbon nanotubes by high temperature annealing, AIP Adv. 3 (2013) 112101, http://dx.doi.org/10.1063/1.4829272.

[37] S.C. Tsang, Y.K. Chen, P.J.F. Harris, M.L.H. Green, A simple chemical method of opening and filling carbon nanotubes, Nature 372 (1994) 159–162, http://dx.doi.org/10.1038/372159a0.

[38] B.C. Satishkumar, A. Govindaraj, J. Mofokeng, G.N. Subbanna, C.N.R. Rao, Novel experiments with carbon nanotubes: opening, filling, closing and functionalizing nanotubes, J. Phys. B At. Mol. Opt. Phys. 29 (1996) 4925–4934, http://dx.doi.org/10.1088/0953-4075/29/21/006.

[39] N. Fischer, E. van Steen, M. Claeys, Preparation of supported nano-sized cobalt oxide and fcc cobalt crystallites, Catal. Today 171 (2011) 174–179, http://dx.doi.org/10.1016/j.cattod.2011.03.018.

[40] Y.J. Wan, J.L. Li, D.H. Chen, Kinetic characterization of the reduction of silica supported cobalt catalysts, J. Therm. Anal. Calorim. 90 (2007) 415–419, http://dx.doi.org/10.1007/s10973-006-7901-y.

[41] B. de Tymowski, Y. Liu, C. Mény, C. Lefevre, D. Begin, P. Nguyen, C. Pham, D. Edouard, F. Luck, C. Pham-Huu, Co–Ru/SiC impregnated with ethanol as an effective catalyst for the Fischer–Tropsch synthesis, Appl. Catal. Gen. 419–420 (2012) 31–40, http://dx.doi.org/10.1016/j.apcata.2012.01.004.

[42] I. Mazov, V.L. Kuznetsov, I.A. Simonova, A.I. Stadnichenko, A.V. Ishchenko, A.I. Romanenko, E.N. Tkachev, O.B. Anikeeva, Oxidation behavior of multiwall carbon nanotubes with different diameters and morphology, Appl. Surf. Sci. 258 (2012) 6272–6280, http://dx.doi.org/10.1016/j.apsusc.2012.03.021.

[43] V.L. (RU) Kuznetsov A.N. (RU) Usol'tseva, Method of producing fine-grained supported catalysts and synthesis of carbon nanotubes, Patent RU 2373995, 2008.

[44] A.S. Andreev, J.-B. d'Espinose de Lacaillerie, O.B. Lapina, A. Gerashenko, Thermal stability and hcp-fcc allotropic transformation in supported Co metal catalysts probed near operando by ferromagnetic NMR, Phys. Chem. Chem. Phys. 17 (2015) 14598–14604, http://dx.doi.org/10.1039/C4CP05327C.

[45] Y. Liu, J. Luo, M. Girleanu, O. Ersen, C. Pham-Huu, C. Meny, Efficient hierarchically structured composites containing cobalt catalyst for clean synthetic fuel production from Fischer–Tropsch synthesis, J. Catal. 318 (2014) 179–192, http://dx.doi.org/10.1016/j.jcat.2014.08.006.

[46] Y. Liu, B. de Tymowski, F. Vigneron, I. Florea, O. Ersen, C. Mény, P. Nguyen, C. Pham, F. Luck, C. Pham-Huu, Titania-decorated silicon carbide-containing cobalt catalyst for Fischer–Tropsch synthesis, ACS Catal. 3 (2013) 393–404,

http://dx.doi.org/10.1021/cs300729p.
[47] Y. Liu, I. Florea, O. Ersen, C. Pham-Huu, C. Meny, Silicon carbide coated with TiO2 with enhanced cobalt active phase dispersion for Fischer–Tropsch synthesis, Chem. Commun. 51 (2015) 145–148, http://dx.doi.org/10.1039/C4CC07469F.
[48] A.S. Andreev, O.B. Lapina, J.-B. d'Espinose de Lacaillerie, A.A. Khassin, Effect of alumina modification on the structure of cobalt-containing Fischer-Tropsch synthesis catalysts according to internal-field 59Co NMR data, J. Struct. Chem. 54 (2013) 102–110, http://dx.doi.org/10.1134/S0022476613070093.
[49] A.S. Andreev, S.F. Tikhov, A.N. Salanov, S.V. Cherepanova, O.B. Lapina, V.A. Bolotov, Y.Y. Tanashev, J.-B. d'Espinose de Lacaillerie, V.A. Sadykov, Design of Al_2O_3/CoAlO/CoAl porous ceramometal for multiple applications as catalytic supports, Adv. Mater. Res. 702 (2013) 79–87 doi:10.4028/www.scientific.net/AMR.702.79.
[50] M. Belesi, I. Panagiotopoulos, S. Pal, S. Hariharan, D. Tsitrouli, G. Papavassiliou, D. Niarchos, N. Boukos, M. Fardis, V. Tzitzios, Decoration of carbon nanotubes with CoO and Co nanoparticles, J. Nanomater 2011 (2011) 1–9, http://dx.doi.org/10.1155/2011/320516.
[51] S.F. Tikhov, A.S. Andreev, A.N. Salanov, S.V. Cherepanova, O.B. Lapina, V.A. Sadykov, Y.Y. Tanashev, V.A. Bolotov, Ceramic matrix composites prepared from CoAl powders, J. Mater. Sci. 51 (2016) 10487–10498, http://dx.doi.org/10.1007/s10853-016-0268-y.
[52] V.L. Kuznetsov, S.N. Bokova-Sirosh, S.I. Moseenkov, A.V. Ishchenko, D.V. Krasnikov, M.A. Kazakova, A.I. Romanenko, E.N. Tkachev, E.D. Obraztsova, Raman spectra for characterization of defective CVD multi-walled carbon nanotubes, Phys. Status Solidi B 251 (2014) 2444–2450, http://dx.doi.org/10.1002/pssb.201451195.
[53] M.A. Shuvaeva, G.S. Litvak, V.A. Varnek, G.A. Bukhtiyarova, Preparation of supported iron-containing catalysts from a FeSo4 solution: the effect of the support, Kinet. Catal. 50 (2009) 874–877, http://dx.doi.org/10.1134/S0023158409060123.
[54] A.S. Andreev, O.B. Lapina, S.V. Cherepanova, A new insight into cobalt metal powder internal field 59Co NMR spectra, Appl. Magn. Reson 45 (2014) 1009–1017, http://dx.doi.org/10.1007/s00723-014-0580-0.
[55] J. Moulijn, A. van Diepen, F. Kapteijn, Catalyst deactivation: is it predictable? Appl. Catal. Gen. 212 (2001) 3–16, http://dx.doi.org/10.1016/S0926-860X(00)00842-5.
[56] J.C. Matsubu, S. Zhang, L. DeRita, N.S. Marinkovic, J.G. Chen, G.W. Graham, X. Pan, P. Christopher, Adsorbate-mediated strong metal–support interactions in oxide-supported Rh catalysts, Nat. Chem. (2016), http://dx.doi.org/10.1038/nchem.2607.
[57] Y. Liu, J. Luo, Y. Shin, S. Moldovan, O. Ersen, A. Hébraud, G. Schlatter, C. Pham-Huu, C. Meny, Sampling the structure and chemical order in assemblies of ferromagnetic nanoparticles by nuclear magnetic resonance, Nat. Commun. 7 (2016) 11532, http://dx.doi.org/10.1038/ncomms11532.
[58] C. de Julián Fernández, Influence of the temperature dependence of anisotropy on the magnetic behavior of nanoparticles, Phys. Rev. B 72 (2005) 054438, http://dx.doi.org/10.1103/PhysRevB.72.054438.
[59] V. Skumryev, S. Stoyanov, Y. Zhang, G. Hadjipanayis, D. Givord, J. Nogués, Beating the superparamagnetic limit with exchange bias, Nature 423 (2003) 850–853, http://dx.doi.org/10.1038/nature01687.
[60] D.L. Leslie-Pelecky, R.D. Rieke, Magnetic properties of nanostructured materials, Chem. Mater. 8 (1996) 1770–1783, http://dx.doi.org/10.1021/cm960077f.
[61] O. Kitakami, H. Sato, Y. Shimada, F. Sato, M. Tanaka, Size effect on the crystal phase of cobalt fine particles, Phys. Rev. B 56 (1997) 13849–13854, http://dx.doi.org/10.1103/PhysRevB.56.13849.
[62] M. Kawakami, T. Hihara, Y. Koi, The Co59 nuclear magnetic resonance in hexagonal cobalt, J. Phys. Soc. Jpn. 33 (1972) 1591–1598.
[63] H.P. Kunkel, C.W. Searle, Experimental identification of domain-wall-center and domain-wall-edge NMR resonances in magnetically ordered materials, Phys. Rev. B 23 (1981) 65–68.
[64] M.A. Kazakova, V.L. Kuznetsov, N.V. Semikolenova, S.I. Moseenkov, D.V. Krasnikov, M.A. Matsko, A.V. Ishchenko, V.A. Zakharov, A.I. Romanenko, O.B. Anikeeva, E.N. Tkachev, V.I. Sushyaev, V.A. Zhuravlev, K.V. Dorozkin, Comparative study of multiwalled carbon nanotube/polyethylene composites produced via different techniques, Phys. Status Solidi B 251 (2014) 2437–2443, http://dx.doi.org/10.1002/pssb.201451194.
[65] A. Aharony, D. Stauffer, Introduction to Percolation Theory, Taylor & Francis, 2003.
[66] D.P. Almond, A.R. West, Impedance and modulus spectroscopy of "real" dispersive conductors, Solid State Ion. 11 (1983) 57–64, http://dx.doi.org/10.1016/0167-2738(83)90063-2.
[67] P. Pötschke, S.M. Dudkin, I. Alig, Dielectric spectroscopy on melt processed polycarbonate—multiwalled carbon nanotube composites, Polymer 44 (2003) 5023–5030, http://dx.doi.org/10.1016/S0032-3861(03)00451-8.
[68] D.J. Bergman, Y. Imry, Critical behavior of the complex dielectric constant near the percolation threshold of a heterogeneous material, Phys. Rev. Lett. 39 (1977) 1222.
[69] J. Zhang, M. Mine, D. Zhu, M. Matsuo, Electrical and dielectric behaviors and their origins in the three-dimensional polyvinyl alcohol/MWCNT composites with low percolation threshold, Carbon 47 (2009) 1311–1320, http://dx.doi.org/10.1016/j.carbon.2009.01.014.
[70] S.I. White, B.A. DiDonna, M. Mu, T.C. Lubensky, K.I. Winey, Simulations and electrical conductivity of percolated networks of finite rods with various degrees of axial alignment, Phys. Rev. B 79 (2009), http://dx.doi.org/10.1103/PhysRevB.79.024301.
[71] J.-X. Liu, H.-Y. Su, D.-P. Sun, B.-Y. Zhang, W.-X. Li, Crystallographic dependence of CO activation on cobalt catalysts: HCP versus FCC, J. Am. Chem. Soc. 135 (2013) 16284–16287, http://dx.doi.org/10.1021/ja408521w.
[72] F. Qin, C. Brosseau, A review and analysis of microwave absorption in polymer composites filled with carbonaceous particles, J. Appl. Phys. 111 (2012) 061301, http://dx.doi.org/10.1063/1.3688435.